



CHORUS

This is the accepted manuscript made available via CHORUS. The article has been published as:

Mott transition in the π -flux SU(4) Hubbard model on a square lattice

Zhichao Zhou, Congjun Wu, and Yu Wang

Phys. Rev. B **97**, 195122 — Published 14 May 2018

DOI: [10.1103/PhysRevB.97.195122](https://doi.org/10.1103/PhysRevB.97.195122)

Mott transition in the π -flux SU(4) Hubbard model on a square lattice

Zhichao Zhou,^{1,2} Congjun Wu,² and Yu Wang^{1,*}

¹*School of Physics and Technology, Wuhan University, Wuhan 430072, China*

²*Department of Physics, University of California, San Diego, CA 92093, USA*

We employ the projector quantum Monte Carlo simulations to study the ground-state properties of the square-lattice SU(4) Hubbard model with a π flux per plaquette. In the weak coupling regime, its ground state is in the gapless Dirac semi-metal phase. With increasing repulsive interaction, we show that, a Mott transition occurs from the semimetal to the valence bond solid, accompanied by the Z_4 discrete symmetry breaking. Our simulations demonstrate the existence of a second-order phase transition, which confirms the Ginzburg-Landau analysis. The phase transition point and the critical exponent η are also estimated. To account for the effect of a π flux on the ordering in the strong coupling regime, we analytically derive by the perturbation theory the ring-exchange term which describes the leading-order difference between the π -flux and zero-flux SU(4) Hubbard models.

I. INTRODUCTION

With the rapid development of ultracold atom experiments, the synthetic gauge field can be implemented in optical lattice systems¹⁻⁴. Recently, the “Hofstadter butterfly” model Hamiltonian has also been achieved with ultracold atoms of ⁸⁷Rb^{5,6}. When ultracold atoms are considered as carriers in optical lattices, they can carry large hyperfine spins. Owing to the closed shell electronic structure of alkaline-earth fermionic atoms, their hyperfine spins are simply nuclear spins, and thus the interatomic scatterings are spin-independent, leading to the SU(2N) symmetry⁷⁻¹¹. A series of experimental breakthroughs have been achieved with SU(2N) ultracold atoms¹²⁻¹⁶. Interestingly, an SU(6) Mott insulating state has been observed with ¹⁷³Yb atoms in the optical lattice¹⁴.

Intense curiosity has been piqued to explore the physics when high symmetry meets the synthetic gauge field. Recent theoretical studies reveal that, the multi-component fermions subject to a gauge field can give rise to the spin liquid phases in the SU(N) Hubbard model at mean-field level¹⁷ as well as in the SU(N) Heisenberg model¹⁸⁻²⁰. In solid state physics, the SU(2N) Heisenberg model was first introduced to handle strong correlation physics by employing the systematic $1/N$ expansion²¹⁻²⁴. The SU(2N) Heisenberg model is often considered as the low-energy effective model of the SU(2N) Hubbard model at strong coupling, where the density fluctuations are neglected. It is found that the filling number of particles per site can strongly affect relevant physics of the SU(2N) Heisenberg model. At quarter filling, its ground state is the long-range antiferromagnetic (AF) order on a square lattice, which is confirmed by various quantum Monte Carlo (QMC) studies²⁵⁻²⁸. At half filling, different QMC methods, however, give rather conflicting results: The AF order was found associated with the ground state by a variational QMC simulation²⁹, whereas neither AF nor dimer orders exist in a projector QMC (PQMC) simulation³⁰.

Considering the significance of density fluctuations in

a realistic fermionic system, the SU(2N) Hubbard model is a prototype model for studying the interplay between density and spin degrees of freedom. The previous PQMC studies of the half-filled SU(2) Hubbard model with a π flux have demonstrated a quantum phase transition from the massless Dirac semimetal phase to a Mott-insulating phase, accompanied by the appearance of the long-range AF ordering³¹⁻³⁵. As for the half-filled SU(4) Hubbard model without a flux, with increasing Hubbard U , the AF order appears on a square lattice,³⁶ while the valence bond solid (VBS) order emerges on a honeycomb lattice³⁷.

The PQMC method is basically unbiased, nonperturbative and asymptotically correct, and particularly sign-problem free at half filling. In this paper, we shall conduct a PQMC study of the ground state properties of the half-filled SU(4) Hubbard model with a π -flux gauge field on a square lattice, which helps to unveil novel physics that is absent in both the SU(2) Hubbard model with a π flux and the SU(4) Hubbard model without a flux. In the noninteracting limit, the ground state of the system is the gapless Dirac semimetal. It is shown that, the increase of the Hubbard U eventually drives the system into a Mott insulating state accompanied by VBS ordering, which breaks the Z_4 discrete symmetry. Since cubic terms are absent in the analytic part of Ginzburg-Landau (GL) free energy, the semimetal-VBS phase transition on a square lattice should be a continuous transition, in contrast to the semimetal-VBS transitions on a honeycomb lattice³⁷⁻⁴¹. Furthermore, the critical exponent η is also extracted by finite size scaling analysis of the numerical data.

The rest of this paper is organized as follows. In Sect. II, the model Hamiltonian and parameters of PQMC simulations are introduced. The Mott gap opening mechanism is then studied in Sect. III. Subsequently in Sect. IV, the nature of quantum phase transitions is investigated. The ring-exchange processes are analyzed in Sect. V. The conclusions are drawn in Sect. VI.

II. MODEL AND METHOD

A. The SU(4) π -flux Hubbard model

The SU(4) Hubbard model at half-filling is defined by the lattice Hamiltonian as

$$H = - \sum_{\langle ij \rangle, \alpha} t_{ij} (c_{i\alpha}^\dagger c_{j\alpha} + h.c.) + \frac{U}{2} \sum_i (n_i - 2)^2 \quad (1)$$

where $\langle ij \rangle$ denotes the nearest neighbors; the sum runs over sites of a square lattice; α represents spin indices running from 1 to 4; n_i is the particle number operator on site i defined as $n_i = \sum_{\alpha=1}^4 c_{i\alpha}^\dagger c_{i\alpha}$ and its average value $\langle n_i \rangle = 2$ in the SU(4) case; U is the on-site repulsive interaction.

For the nearest-neighbor hopping integral t_{ij} , we use the following gauge that $t_x = t$ and $t_y = (-1)^x t$, such that the product of phases of hopping integrals around a plaquette is $e^{i\pi} = -1$ as illustrated in Fig.1(a). At weak coupling, the low-energy effective theory of the π -flux model on a square lattice can be formulated in terms of Dirac fermions. In the weak coupling limit of $U/t \rightarrow 0$, the dispersion relations are $\varepsilon(\vec{k}) = \pm 2t \sqrt{\cos^2(k_x) + \cos^2(k_y)}$, hence there exist eight low-energy Dirac cones located at $(\pm \frac{\pi}{2}, \pm \frac{\pi}{2})$ when taking into account the spin degeneracy, as shown in Fig.1(b). In the atomic limit of $U/t \rightarrow \infty$, the system is in the Mott-insulating states at half-filling. If a single particle is removed from one site and added to another site, the excitation energy is U , independent of the fermion components.

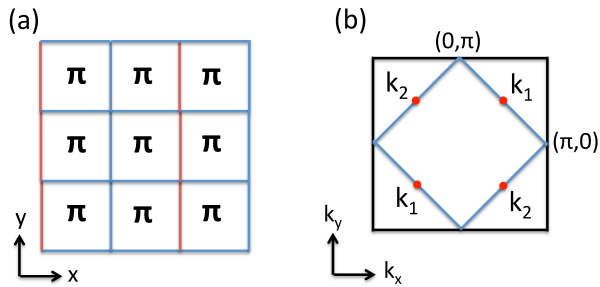


FIG. 1. (a) The hopping integrals on a square lattice. Red and blue lines correspond to $-t$ and t , respectively, hence each plaquette is penetrated by a π flux. (b) The Brillouin zone of the π -flux model on a square lattice. The blue lines depict the Fermi surface at half-filling in the absence of flux. The red points are the Dirac points at $\vec{k}_{1,2} = (\frac{\pi}{2}, \pm \frac{\pi}{2})$, and the points of $(\pm \frac{\pi}{2}, \frac{\pi}{2})$ are equivalent to $\vec{k}_{1,2}$.

B. Parameters of PQMC simulations

We shall employ the zero-temperature PQMC method in the determinant formalism^{42–44}. Recently, exciting progress has been achieved in the PQMC algorithm for

the sign-problem free simulations^{45–48}. For this square-lattice SU(4) Hubbard model with a π -flux gauge field, the Kramers positive decomposition guarantees the absence of sign problem at half filling⁴⁵.

To simulate the π -flux model, the square lattice in real space is subject to the periodic boundary condition for $L = 4n$ and the anti-periodic boundary condition for $L = 4n + 2$, where n is an integer³³. The trial wave function is chosen as the ground state wavefunction of the noninteracting part of Eq.[1] with a small flux added for lifting the degeneracy at the Dirac points. The simulation parameters are set to $\Delta\tau = 0.05$ and $\beta = 40$. The measurements of physical observables are performed around $\beta/2$ after projecting onto the ground state.

III. GAP OPENING MECHANISM

In the weak coupling regime, the system lies in the semimetal phase. With the increase of the coupling strength U , the system undergoes a phase transition from semimetal to Mott-insulating phase. In the SU(2) case, this transition is well-studied by the QMC method^{31–35}. In the absence of intermediate spin liquid phase, a second-order phase transition occurs from the Dirac semimetal phase to the AF phase. Nevertheless, the ordering of Mott insulating phase in the SU(4) case remains unclear.

A. Single-particle gap opening

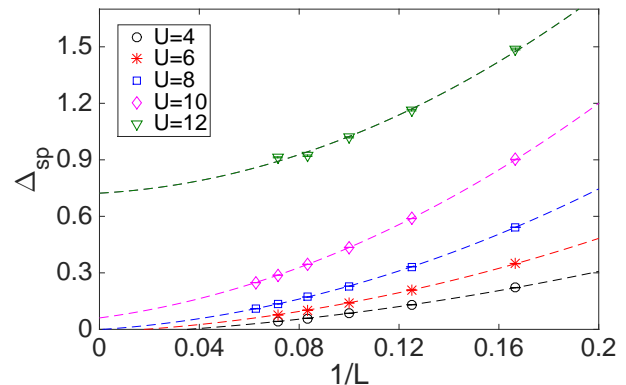


FIG. 2. The finite-size scalings of the single-particle gap Δ_{sp} for the SU(4) π -flux Hubbard model as the Hubbard U varies. The quadratic polynomial fitting is used. Error bars are smaller than symbols.

Since the Dirac cones are located at $\vec{k}_{1,2} = (\frac{\pi}{2}, \pm \frac{\pi}{2})$, we use the PQMC method to calculate the unequal-time Green's function from which the single-particle gap Δ_{sp} at $\vec{k}_{1,2}$ can be extracted for various U . Then the parameter regime of the Mott-insulating phase can be determined accordingly. By the finite-size scalings, we find

that, the critical coupling strength U_c for single-particle gap opening lies in the range from 8 to 10, as shown in Fig. 2. This value of U_c lies in between the critical couplings of π -flux model with $SU(2)$ symmetry and the $SU(4)$ honeycomb-lattice Hubbard model with zero flux. $U_c/t \approx 5.5$ in the former case^{34,35}, while $U_c/t \approx 7$ in the latter case³⁷. This difference can be understood with the intuitive picture as follows^{37,49}. In the atomic limit $U/t \rightarrow \infty$, the single particle gap $\Delta_{sp} = U/2$, which represents the energy barrier for adding one more fermion to the Mott-insulating background. After the hopping is switched on, the number of hopping processes is proportional to zN , which results in the band width $W \approx 2zNt$. The single-particle gap can therefore be estimated by the relation

$$\Delta_{sp} \approx \frac{U}{2} - zNt, \quad (2)$$

which implies $U_c/t \approx 2zN$. Physically speaking, both the multi components and the increase of coordinate number can enhance the hopping processes, which suppresses the single-particle gap Δ_{sp} and thus lead to the increase of the critical coupling U_c . This argument is quantitatively consistent with our PQMC results.

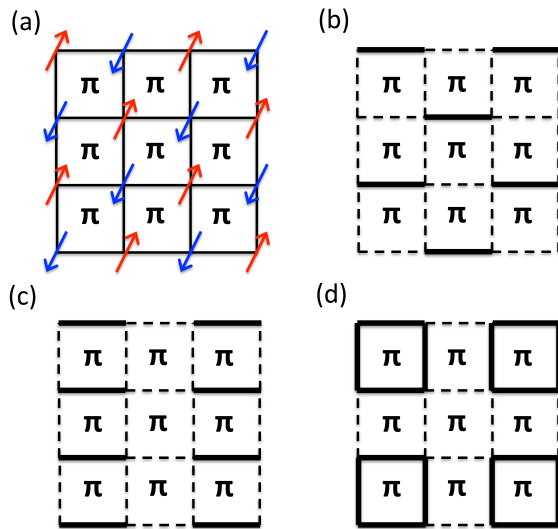


FIG. 3. Possible configurations of ordering: (a) AF order; (b) Staggered VBS order; (c) Columnar VBS order; (d) Plaquette VBS order.

B. The antiferromagnetic (AF) ordering

Generally, the equal-time $SU(2N)$ spin-spin correlation function can be defined as

$$S_{spin}(i, j) = \sum_{\alpha, \beta} S_{\alpha\beta}(i) \cdot S_{\beta\alpha}(j), \quad (3)$$

where $S_{\alpha\beta}(i) = c_{i,\alpha}^\dagger c_{i,\beta} - \frac{\delta^{\alpha\beta}}{2N} \sum_{\gamma=1}^{2N} c_{i,\gamma}^\dagger c_{i,\gamma}$ are the generators of an $SU(2N)$ group obeying the commutation

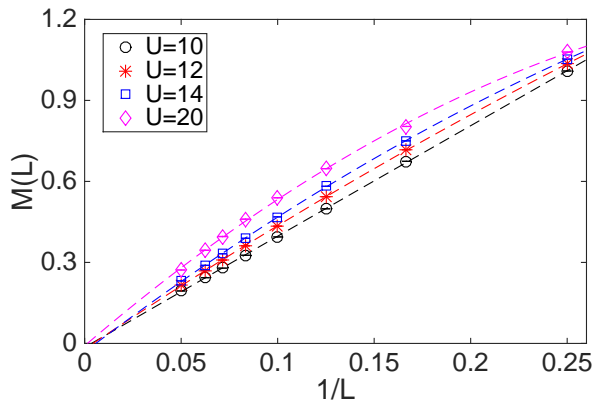


FIG. 4. Finite-size scalings of the AF order parameter $M(L)$ versus $1/L$ as U varies in the π -flux $SU(4)$ Hubbard model. The quadratic polynomial fitting is used. Error bars are smaller than symbols.

relation $[S_{\alpha\beta}, S_{\gamma\delta}] = \delta^{\beta\gamma} S_{\alpha\delta} - \delta^{\alpha\delta} S_{\gamma\beta}$. The spin structure factor is defined in terms of the spin-spin correlation function as follows:

$$S_{su(2N)}(\vec{q}) = \frac{1}{L^2} \sum_{i,j} e^{i\vec{q}\cdot\vec{r}} S_{spin}(i, j), \quad (4)$$

where \vec{r} is the relative vector between sites i and j . Then the $SU(2N)$ long-range AF order is given by the relation

$$M = \lim_{L \rightarrow \infty} \sqrt{\frac{1}{L^2} S_{su(2N)}(\vec{Q})} \quad (5)$$

with $\vec{Q} = (\pi, \pi)$.

Previous PQMC studies of the π -flux $SU(2)$ model³¹⁻³⁵ indicate that the ground state of the $SU(2)$ Mott insulator is associated with the AF order. In the zero-flux $SU(4)$ Hubbard model³⁶, the AF order appears starting from the weak coupling regime, and exhibits a non-monotonic behavior as the interaction strength varies. It first increases with the interaction strength U , and then after reaching a maximal value at $U/t \approx 8$, it begins to be suppressed by quantum spin fluctuations as U further increases. The AF order still persists even at $U/t = 20$, while it remains unclear whether it can be suppressed to zero in the limit of $U \rightarrow \infty$.

Our simulations of the π -flux $SU(4)$ model, in contrast, demonstrate that the long-range AF order is absent in the Mott-insulating state. For our case, the finite-size scalings of the AF order parameter $M(L)$ is presented in Fig.4. Although $M(L)$ increases with the Hubbard U , the scaling results at $L \rightarrow \infty$ show that the long-range AF order M vanishes even at $U/t = 20$. In particular, the curvatures of these $M(L)$ curves are negative and thus it is conceivable that they converge to zero as $L \rightarrow \infty$. It is seen that both the multi-flavors of fermion species and the π flux suppress the AF ordering.

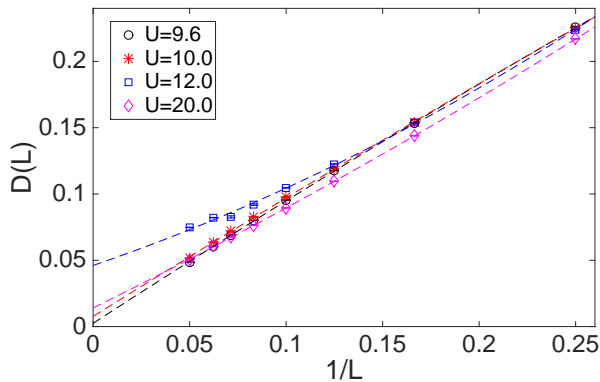


FIG. 5. Finite-size scalings of $D(L)$ versus $1/L$ as U varies in the π -flux SU(4) Hubbard model. The quadratic polynomial fitting is used. Error bars are smaller than symbols.

C. The VBS order

In this part, we analyze the VBS ordering pattern on a square lattice for the π -flux SU(4) Hubbard model. Generally speaking, for the staggered VBS order as depicted in Fig. 3(b), its wavevector remains at (π, π) and does not break extra symmetries, hence, the locations of the Dirac cones are shifted but still exist⁵⁰. In order to open gaps, we shall consider the columnar VBS (cVBS) order and plaquette VBS (pVBS) order as depicted in Figs. 3(c) and 3(d), respectively. They only differ in the structure of a phase factor⁵¹.

Following Ref.[51], we define a gauge-invariant VBS order below. First, the nearest-neighboring bonds d_{i, \hat{e}_j} are defined via the kinetic energy:

$$d_{i, \hat{e}_j} = \frac{1}{2N} \sum_{\alpha=1}^{2N} (c_{i, \alpha}^\dagger t_{i, i+\hat{e}_j} c_{i+\hat{e}_j, \alpha} + h.c.), \quad (6)$$

where \hat{e}_j ($j = 1, 2$) are two basis vectors of the square lattice. Then the structure factors of the VBS along the x and y directions are defined as

$$\begin{aligned} \chi_x(L, \vec{q}_{x0}) &= \frac{1}{L^A} \sum_{ij} d_{i, \hat{e}_x} d_{j, \hat{e}_x} e^{i\vec{q}_x \cdot \vec{r}} \\ \chi_y(L, \vec{q}_{y0}) &= \frac{1}{L^A} \sum_{ij} d_{i, \hat{e}_y} d_{j, \hat{e}_y} e^{i\vec{q}_y \cdot \vec{r}} \end{aligned} \quad (7)$$

where $\vec{q}_x = (\pi, 0)$, $\vec{q}_y = (0, \pi)$, and \vec{r} is the relative vector between sites i and j . The strength of the VBS order parameter is thus expressed as

$$D = \lim_{L \rightarrow +\infty} \sqrt{\chi_x(L, \vec{q}_{x0}) + \chi_y(L, \vec{q}_{y0})}. \quad (8)$$

In principle, the probability distribution of χ_x and χ_y can be used to further distinguish the cVBS and pVBS ordering on a square lattice. They exhibit different Z_4 symmetry breaking patterns: For the cVBS ordering, the peaks of $P(\chi_x, \chi_y)$ are located at the angles of $0, \frac{\pi}{2}, \pi, \frac{3\pi}{2}$,

while for the pVBS ordering, its peaks are located at direction of $\frac{\pi}{4}, \frac{3\pi}{4}, \frac{5\pi}{4}, \frac{7\pi}{4}$. However, given the lattice size studied in our simulations, it is hard to distinguish the cVBS and pVBS orders by $P(\chi_x, \chi_y)$.

In Fig. 5, the finite size scalings of the VBS order $D(L)$ are presented. With the Mott gap opening, the long-range VBS order starts to appear at around $U/t \approx 9$. In the next section, the phase transition point is to be determined more accurately by calculating the Binder ratios. Due to the suppression of the overall kinetic energy scale, the U -dependence of VBS order is non-monotonic³⁷. Moreover, this non-monotonic behavior cannot be regarded as a signal of the suppression of VBS order by other competing orders.

IV. NATURE OF THE MOTT TRANSITION

Recently, large-scale QMC simulations have been widely employed to investigate critical phenomena of a lattice model. For example, the spinless Dirac fermions on a honeycomb and a π -flux square lattices undergo a quantum phase transition to the charge density wave (CDW) order with increasing nearest-neighboring repulsion V ⁵²⁻⁵⁴. This semimetal-CDW transition belongs to the chiral Ising universality class due to the fact that CDW ordering breaks the discrete sublattice symmetry⁵². In both the SU(2) honeycomb-lattice and the SU(2) π -flux square-lattice Hubbard models, increasing U triggers the semimetal-AF phase transition, which belongs to the chiral Heisenberg universality class^{34,35}. However, the Mott transitions of the SU(4) Dirac fermions are different on the honeycomb lattice and π -flux square lattice. In both models, with increasing Hubbard U , the SU(4) Dirac fermions undergo a semimetal-VBS phase transition. The Mott transition breaks the Z_3 symmetry on a honeycomb lattice³⁷, while the Z_4 symmetry is broken on a π -flux square lattice.

On the honeycomb lattice, the analytic part of the Ginzburg-Landau (GL) free energy contains a cubic term allowed by the Z_3 symmetry. Hence, generally speaking, the semimetal-VBS phase transition on a honeycomb lattice should be of first order^{37,55}. However the coupling of VBS to Dirac fermions can soften the phase transition to the second order³⁷⁻⁴¹. On a square lattice with a π flux, the VBS order breaks the Z_4 symmetry, and consequently the cubic term is not allowed in the analytic part of GL free energy. Along the same line of Ref. [37], we can evaluate the nonanalytic part of the GL free energy by tracing out the degrees of freedom of SU(2N) Dirac fermions. At the mean-field level, the free-energy density that may contribute the cubic term at half filling is

$$f \approx -\frac{1}{\beta} \int_0^\Lambda \frac{d^2 \vec{k}}{(2\pi)^2} \ln[(1 + e^{\beta E_k})(1 + e^{-\beta E_k})]^{4N}, \quad (9)$$

where $E_k = \sqrt{v^2 k^2 + |\psi|^2}$ is the single-particle spectrum around each Dirac cone, and $|\psi|$ is the gap function of the VBS order at the mean-field level; β is the

inverse temperature, and Λ is the momentum cutoff. In the low-temperature limit, we have

$$\begin{aligned} \lim_{\beta \rightarrow \infty} f &= -4N \int_0^\Lambda \frac{dk_x dk_y}{4\pi^2} \sqrt{v^2 k^2 + |\psi|^2} \\ &= -\frac{2N}{3\pi v^2} [(\Lambda^2 v^2 + |\psi|^2)^{3/2} - |\psi|^3]. \end{aligned} \quad (10)$$

We perform the Taylor expansion of the right-hand side of this equation at the critical point where $|\psi| \rightarrow 0$, and then find a non-analytic cubic term below

$$f_{cubic} = \frac{2N}{3\pi v^2} |\psi|^3 > 0. \quad (11)$$

It implies that, the semimetal-VBS phase transition on a π -flux square lattice should be of the second order. This type of quantum phase transition can be investigated by the finite-size scalings of the numerical data.

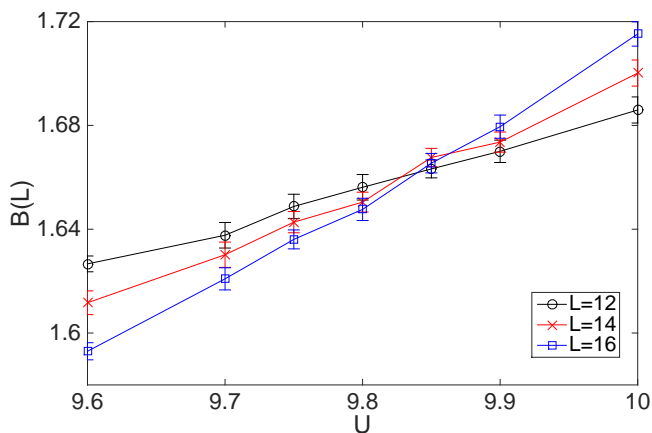


FIG. 6. Binder ratios $B(L)$ for semimetal-VBS transition with different U and L . The crossing point suggests a critical value in between $U = 9.8 \sim 9.9$.

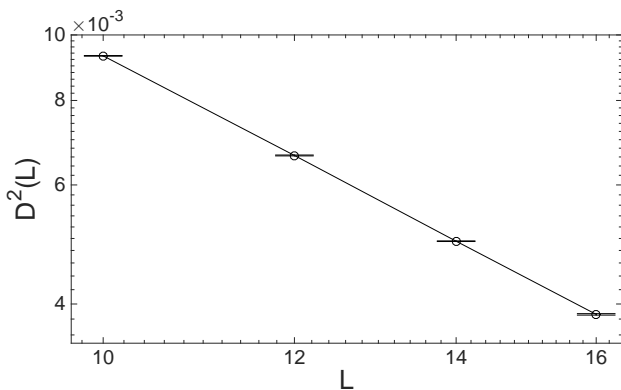


FIG. 7. Critical scaling behavior of the VBS order parameter $D^2(L)$ versus the lattice size L at $U/t = 9.8$. The critical exponent $z + \eta$ can be extracted from the slope of the log-log plot of the $D^2(L) - L$ curve.

In order to locate the phase transition point more accurately, we define the Binder ratios as follow^{34,38,56}. For χ_x , we define $\vec{q}_x = (\pi, 0)$, $\vec{q}_{x_1} = (\pi + \frac{2\pi}{L}, 0)$, and $\vec{q}_{x_2} = (\pi, \frac{2\pi}{L})$. Then we have the binder ratios parallel and perpendicular to the x bonds on the $L \times L$ lattice,

$$B_1^x(L) = \frac{\chi_x(L, \vec{q}_x)}{\chi_x(L, \vec{q}_{x_1})}, \quad B_2^x(L) = \frac{\chi_x(L, \vec{q}_x)}{\chi_x(L, \vec{q}_{x_2})}. \quad (12)$$

Similarly for χ_y , we define $\vec{q}_y = (0, \pi)$, $\vec{q}_{y_1} = (\frac{2\pi}{L}, \pi)$, and $\vec{q}_{y_2} = (0, \pi + \frac{2\pi}{L})$. Then we have the Binder ratios perpendicular and parallel to the y bonds on the $L \times L$ lattice,

$$B_1^y(L) = \frac{\chi_y(L, \vec{q}_y)}{\chi_y(L, \vec{q}_{y_1})}, \quad B_2^y(L) = \frac{\chi_y(L, \vec{q}_y)}{\chi_y(L, \vec{q}_{y_2})}. \quad (13)$$

At the critical point of the second-order phase transition, the Binder ratio should reach a size-independent value as the lattice size L grows. According to this principle, the critical coupling U_c can be determined in Fig.6, where $B(L) = \frac{1}{4}[B_1^x(L) + B_2^x(L) + B_1^y(L) + B_2^y(L)]$ is a arithmetic average. The crossing point in Fig.6 indicates a second-order phase transition with a critical coupling in between $U = 9.8$ and $U = 9.9$. Then we assume the VBS order obeys the following scaling ansatz⁵⁷⁻⁵⁹

$$D^2(L) = L^{-z-\eta} \mathcal{F}[(U - U_c)L^{1/\nu}]. \quad (14)$$

where η and ν are dimensionless critical exponents; z is the dynamic exponent; \mathcal{F} is the scaling function. As shown in Fig.7, the critical exponent η can be extracted from the slope of the log-log plot of the $D^2(L) - L$ curve in the critical region $U = 9.8 \sim 9.9$. η is found to be 0.86 ± 0.04 via the linear fitting with the assumption of $z = 1$. Due to the limitation of the lattice size that we can simulate, the critical exponent of ν can not be extracted by data collapse.

V. THE RING-EXCHANGE PROCESS

The above QMC results show the semimetal to the VBS transition in the π -flux SU(4) Hubbard model on a square lattice, and the absence of AF ordering even at $U/t = 20$. In contrast, it has been shown in the previous work that the ground state of the zero-flux SU(4) Hubbard model on a square lattice is associated with the AF order³⁶, which depends on U non-monotonically. Until now, physics in the large- U limit for both the zero-flux and π -flux half-filled SU(4) Hubbard models on a square lattice is still an open question.

In fact, in the strong coupling regime, both the zero-flux and π -flux SU(4) Hubbard models, to the 2nd-order perturbation, identically reduce to the SU(4) Heisenberg model with the single column self-conjugate representation. The differences between the zero-flux and π -flux Hubbard models arise from the higher order perturbation

terms, for example, the next higher-order contributions from the four-site ring-exchange term.

The four-site ring-exchange terms can be expressed as follows,

$$H^{(4)}(\square) = -\frac{1}{U^3}T_{-1}T_0T_0T_{+1} - \frac{1}{2U^3}T_{-1}T_{-1}T_{+1}T_{+1}, \quad (15)$$

where T_m corresponds to the hopping process that changes the interaction energy by mU . For the SU(4) case, $m = -3$ to 3 . (See Appendix A for details.) The four-site ring-exchange process describes that fermions hop along a linked loop in a plaquette. Unlike the zero-flux case, fermions in the π -flux model gain an additional π phase once they experience the ring-exchange process. As a result, the four-site ring-exchange terms of the zero-flux and π -flux models have opposite signs.

We speculate that the different four-site ring-exchange terms are responsible for the different orderings in the Mott-insulating phase in the strong coupling regime. Previous QMC simulations of the SU(4) Heisenberg model with the single-column self-conjugate representation on a square lattice show the evidence of a gapless spin liquid. It would be interesting to check if the SU(4) Heisenberg model is critical. If it is the case, then it will be reasonable to speculate that the four-site ring-exchange terms stabilize orderings of VBS and AF in the π -flux and zero-flux cases, respectively, depending on the signs of the ring-exchange terms.

VI. CONCLUSIONS AND DISCUSSIONS

In summary, we have employed the PQMC simulations to study the ground-state properties of the π -flux square-lattice SU(4) Hubbard model. At the critical coupling in between $U = 9.8$ and $U = 9.9$, the SU(4) Dirac fermions on the square lattice undergo a Mott transition to the VBS, which breaks the Z_4 discrete symmetry. The GL free energy is free of the cubic term, while its non-analytic part contains the term of $|\psi|^3$ with a positive coefficient, which implies that the semimetal-VBS transition is of second order. The nonperturbative PQMC simulations also prove the existence of a second-order phase transition with critical exponent $\eta = 0.86 \pm 0.04$.

Our work demonstrates that the combination of the SU(4) symmetry and the π flux dramatically affects the quantum phase transitions on a square lattice. Compared with the π -flux SU(2) and the zero-flux SU(4) models, at the even stronger critical coupling U_c the π -flux SU(4) model undergoes a Mott transition to a VBS order rather than an AF order. Due to Fermi surface nesting, the zero-flux SU(4) model enters Mott-insulating state at infinitesimal coupling. The multiple fermion components enhance the charge fluctuations, which increases the critical coupling for the emergence of a Mott insulator. In the presence of a π flux, stronger spin fluctuations entirely suppress the AF ordering, and instead the VBS order

emerges in the SU(4) Mott-insulating state. SU(4) Dirac fermions on the square lattice energetically favor VBS order rather than the AF order in the strong coupling regime, which is consistent with the behavior of SU(2N) Dirac fermions studied on a honeycomb lattice³⁷. To account for the effect of a π flux on the ordering in the strong coupling regime, we analytically derive by perturbation theory the ring-exchange term which describes the leading-order difference between the π -flux and zero-flux SU(4) Hubbard models. The ring-exchange terms for the two cases differ a minus sign. However a definite proof of the physical consequence of the ring-exchange term requires further study.

ACKNOWLEDGMENTS

This work is financially supported by the National Natural Science Foundation of China under Grant Nos. 11729402, 11574238, and 11328403. Z. Z. and Y. W. are grateful for the award of scholarships funded by the China Scholarship Council (File Nos. 201606270067 and 201706275082). C. W. is supported by the AFOSR FA9550-14-1-0168. This work made use of the facilities of Tianhe-2 at the China's National Supercomputing Centre in Guangzhou. Z.Z. and Y.W. also acknowledge the support of the Supercomputing Center of Wuhan University.

Appendix A: Canonical transformation of the SU(4) Hubbard Hamiltonian in the strong coupling limit

The original Hamiltonian Eq.[1] can be written in the form

$$H = \sum_{m=-3}^3 T_m + V, \quad (A1)$$

where V is the interaction term

$$V = U \sum_i \sum_{\alpha \neq \beta} n_{i\alpha} n_{i\beta}. \quad (A2)$$

and T_m is associated with the hopping process that changes the interaction energy by mU . For SU(4) case, $m = -3, -2, -1, 0, 1, 2, 3$. T_m can be explicitly expressed in terms of the projection operator $P_i^\alpha(n)$ for site i below

$$\begin{aligned} P_i^\alpha(0) &= \prod_{\beta \neq \alpha} (1 - n_{i\beta}), \\ P_i^\alpha(1) &= \sum_{\beta \neq \alpha} (n_{i\beta}) \prod_{\gamma \neq \alpha, \beta} (1 - n_{i\gamma}), \\ P_i^\alpha(2) &= \sum_{\beta \neq \alpha} (1 - n_{i\beta}) \prod_{\gamma \neq \alpha, \beta} (n_{i\gamma}), \\ P_i^\alpha(3) &= \prod_{\beta \neq \alpha} (n_{i\beta}). \end{aligned} \quad (A3)$$

Then the hopping terms are

$$\begin{aligned}
T_{+3} &= - \sum_{\langle i,j \rangle; \alpha} t_{ij} [P_i^\alpha(3) c_{i\alpha}^\dagger c_{j\alpha} P_j^\alpha(0)], \\
T_{+2} &= - \sum_{\langle i,j \rangle; \alpha} t_{ij} \sum_{n=0}^1 [P_i^\alpha(n+2) c_{i\alpha}^\dagger c_{j\alpha} P_j^\alpha(n)], \\
T_{+1} &= - \sum_{\langle i,j \rangle; \alpha} t_{ij} \sum_{n=0}^2 [P_i^\alpha(n+1) c_{i\alpha}^\dagger c_{j\alpha} P_j^\alpha(n)], \\
T_0 &= - \sum_{\langle i,j \rangle; \alpha} t_{ij} \sum_{n=0}^3 [P_i^\alpha(n) c_{i\alpha}^\dagger c_{j\alpha} P_j^\alpha(n)], \quad (A4)
\end{aligned}$$

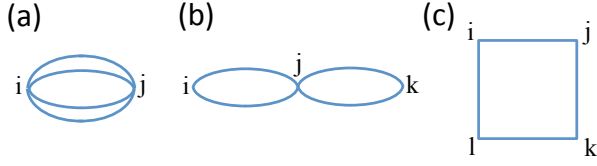


FIG. 8. The hopping process corresponding to the 4th-order perturbation term links (a) two, (b) three, or (c) four lattice sites.

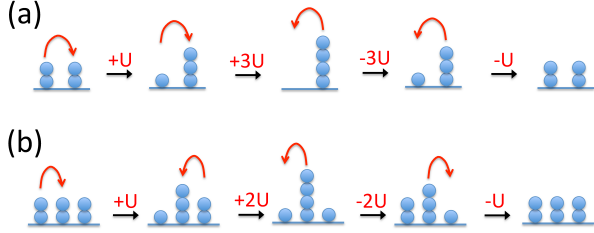


FIG. 9. (a) Hopping process $T_{-1}T_{-3}T_{+3}T_{+1}$ only occurs on two-site configurations. (b) Hopping process $T_{-1}T_{-2}T_{+2}T_{+1}$ only occurs on three-site configurations.

In the strong coupling limit of $|U/t| \rightarrow \infty$, the Hamiltonian can be block diagonalized such that the interaction energy $\langle V \rangle$ is constant in each block with hopping processes serving as perturbations. For the block diagonalization of the Hamiltonian, a canonical transformation $H' = e^{iS} H e^{-iS}$ is performed to eliminate hopping between blocks associated with different $\langle V \rangle$ ⁶⁰. The perturbation terms can be formed as a product of hopping T_m 's. The 0th-order perturbation reads

$$H'^{(0)} = V + T_0. \quad (A5)$$

At half filling, the 2nd-order and 4th-order perturbations can be written as,

$$H'^{(2)} = -\frac{1}{U} T_{-1} T_{+1}, \quad (A6)$$

$$\begin{aligned}
H'^{(4)} &= + \frac{1}{U^3} T_{-1} T_{+1} T_{-1} T_{+1} \\
&\quad - \frac{1}{U^3} T_{-1} T_0 T_0 T_{+1} \\
&\quad - \frac{1}{2U^3} T_{-1} T_{-1} T_{+1} T_{+1} \\
&\quad - \frac{1}{3U^3} T_{-1} T_{-2} T_{+2} T_{+1} \\
&\quad - \frac{1}{4U^3} T_{-1} T_{-3} T_{+3} T_{+1}. \quad (A7)
\end{aligned}$$

The 2nd-order perturbation just involves the two-site hopping process, and can be mapped to the SU(4) Heisenberg model in the self-conjugate representation^{61,62}. As shown in Fig.8, the 4th-order perturbation corresponds to three different linked hopping processes, in which the hopping process $T_{-1}T_{-3}T_{+3}T_{+1}$ (Fig.9(a)), $T_{-1}T_{-2}T_{+2}T_{+1}$ (Fig.9(b)), and $T_{-1}T_{+1}T_{-1}T_{+1}$ do not describe the ring-exchange process on a four-site plaquette (Fig.8(c))⁶³. Consequently, the ring-exchange process can be written as Eq.[15] in the main text.

* yu.wang@whu.edu.cn

¹ D. Jaksch and P. Zoller, *New Journal of Physics* **5**, 56 (2003).
² J. Dalibard, F. Gerbier, G. Juzeliūnas, and P. Öhberg, *Rev. Mod. Phys.* **83**, 1523 (2011).
³ N. Goldman, G. Juzeliūnas, P. Öhberg, and I. B. Spielman, *Reports on Progress in Physics* **77**, 126401 (2014).
⁴ E. Zohar, J. I. Cirac, and B. Reznik, *Reports on Progress in Physics* **79**, 014401 (2015).
⁵ H. Miyake, G. A. Siviloglou, C. J. Kennedy, W. C. Burton, and W. Ketterle, *Phys. Rev. Lett.* **111**, 185302 (2013).
⁶ M. Aidelsburger, M. Atala, M. Lohse, J. T. Barreiro, B. Paredes, and I. Bloch, *Phys. Rev. Lett.* **111**, 185301 (2013).
⁷ C. Wu, J. P. Hu, and S. C. Zhang, *Phys. Rev. Lett.* **91**, 186402 (2003).
⁸ C. Honerkamp and W. Hofstetter, *Phys. Rev. Lett.* **92**,

170403 (2004).

⁹ C. Wu, *Phys. Rev. Lett.* **95**, 266404 (2005).
¹⁰ C. Wu, *Mod. Phys. Lett. B* **20**, 1707 (2006).
¹¹ A. V. Gorshkov, M. Hermele, V. Gurarie, C. Xu, P. S. Julienne, J. Ye, P. Zoller, E. Demler, M. D. Lukin, and A. M. Rey, *Nature Phys.* **6**, 289 (2010).
¹² S. Taie, Y. Takasu, S. Sugawa, R. Yamazaki, T. Tsujimoto, R. Murakami, and Y. Takahashi, *Phys. Rev. Lett.* **105**, 190401 (2010).
¹³ B. J. DeSalvo, M. Yan, P. G. Mickelson, Y. N. Martinez de Escobar, and T. C. Killian, *Phys. Rev. Lett.* **105**, 030402 (2010).
¹⁴ S. Taie, R. Yamazaki, S. Sugawa, and Y. Takahashi, *Nature Physics* **8**, 825 (2012).
¹⁵ G. Pagano, M. Mancini, G. Cappellini, P. Lombardi, F. Schiffrer, H. Hu, X.-J. Liu, J. Catani, C. Sias, M. Inguscio, and L. Fallani, *Nat. Phys.* **10**, 198 (2014).

- ¹⁶ C. Hofrichter, L. Riegger, F. Scazza, M. Höfer, D. R. Fernandes, I. Bloch, and S. Fölling, *Phys. Rev. X* **6**, 021030 (2016).
- ¹⁷ G. Chen, K. R. A. Hazzard, A. M. Rey, and M. Hermele, *Phys. Rev. A* **93**, 061601 (2016).
- ¹⁸ M. Hermele, V. Gurarie, and A. M. Rey, *Phys. Rev. Lett.* **103**, 135301 (2009).
- ¹⁹ M. Hermele and V. Gurarie, *Phys. Rev. B* **84**, 174441 (2011).
- ²⁰ P. Nataf, M. Lajkó, A. Wietek, K. Penc, F. Mila, and A. M. Läuchli, *Phys. Rev. Lett.* **117**, 167202 (2016).
- ²¹ I. Affleck, *Phys. Rev. Lett.* **54**, 966 (1985).
- ²² D. P. Arovas and A. Auerbach, *Phys. Rev. B* **38**, 316 (1988).
- ²³ I. Affleck and J. B. Marston, *Phys. Rev. B* **37**, 3774 (1988).
- ²⁴ N. Read and S. Sachdev, *Nucl. Phys. B* **316**, 609 (1989).
- ²⁵ K. Harada, N. Kawashima, and M. Troyer, *Phys. Rev. Lett.* **90**, 117203 (2003).
- ²⁶ N. Kawashima and Y. Tanabe, *Phys. Rev. Lett.* **98**, 057202 (2007).
- ²⁷ K. S. D. Beach, F. Alet, M. Mambrini, and S. Capponi, *Phys. Rev. B* **80**, 184401 (2009).
- ²⁸ R. K. Kaul and A. W. Sandvik, *Phys. Rev. Lett.* **108**, 137201 (2012).
- ²⁹ A. Paramekanti and J. B. Marston, *J. Phys. Cond. Matt.* **19**, 125215 (2007).
- ³⁰ F. F. Assaad, *Phys. Rev. B* **71**, 75103 (2005).
- ³¹ Y. Otsuka and Y. Hatsugai, *Phys. Rev. B* **65**, 073101 (2002).
- ³² C.-C. Chang and R. T. Scalettar, *Phys. Rev. Lett.* **109**, 026404 (2012).
- ³³ Y. Otsuka, S. Yunoki, and S. Sorella, “Mott transition in the 2d hubbard model with π -flux,” in *Proceedings of the International Conference on Strongly Correlated Electron Systems (SCES)*, <http://journals.jps.jp/doi/pdf/10.7566/JPSCP.3.013021>.
- ³⁴ F. Parisen Toldin, M. Hohenadler, F. F. Assaad, and I. F. Herbut, *Phys. Rev. B* **91**, 165108 (2015).
- ³⁵ Y. Otsuka, S. Yunoki, and S. Sorella, *Phys. Rev. X* **6**, 011029 (2016).
- ³⁶ D. Wang, Y. Li, Z. Cai, Z. Zhou, Y. Wang, and C. Wu, *Phys. Rev. Lett.* **112**, 156403 (2014).
- ³⁷ Z. Zhou, D. Wang, Z. Y. Meng, Y. Wang, and C. Wu, *Phys. Rev. B* **93**, 245157 (2016).
- ³⁸ Z.-X. Li, Y.-F. Jiang, S.-K. Jian, and H. Yao, arXiv:1512.07908 (2015).
- ³⁹ S.-K. Jian and H. Yao, arXiv:1610.07603 (2016).
- ⁴⁰ M. M. Scherer and I. F. Herbut, *Phys. Rev. B* **94**, 205136 (2016).
- ⁴¹ L. Classen, I. F. Herbut, and M. M. Scherer, arXiv:1705.08973 (2017).
- ⁴² R. Blankenbecler, D. J. Scalapino, and R. L. Sugar, *Phys. Rev. D* **24**, 2278 (1981).
- ⁴³ J. E. Hirsch, *Phys. Rev. B* **31**, 4403 (1985).
- ⁴⁴ F. Assaad and H. Evertz, *Computational Many-Particle Physics* (Lect. Notes Phys. 739, Springer, 2008) p. 277.
- ⁴⁵ C. Wu and S. C. Zhang, *Phys. Rev. B* **71**, 155115 (2005).
- ⁴⁶ L. Wang, Y.-H. Liu, M. Iazzi, M. Troyer, and G. Harcos, *Phys. Rev. Lett.* **115**, 250601 (2015).
- ⁴⁷ Z. C. Wei, C. Wu, Y. Li, S. Zhang, and T. Xiang, *Phys. Rev. Lett.* **116**, 250601 (2016).
- ⁴⁸ Z.-X. Li, Y.-F. Jiang, and H. Yao, *Phys. Rev. Lett.* **117**, 267002 (2016).
- ⁴⁹ Z. Zhou, Z. Cai, C. Wu, and Y. Wang, *Phys. Rev. B* **90**, 235139 (2014).
- ⁵⁰ D. Ixert, F. F. Assaad, and K. P. Schmidt, *Phys. Rev. B* **90**, 195133 (2014).
- ⁵¹ A. W. Sandvik, in *AIP Conference Proceedings*, Vol. 1297 (AIP, 2010) pp. 135–338.
- ⁵² L. Wang, P. Corboz, and M. Troyer, *New Journal of Physics* **16**, 103008 (2014).
- ⁵³ Z.-X. Li, Y.-F. Jiang, and H. Yao, *Phys. Rev. B* **91**, 241117 (2015).
- ⁵⁴ Z.-X. Li, Y.-F. Jiang, and H. Yao, *New Journal of Physics* **17**, 085003 (2015).
- ⁵⁵ J. Motruk, A. G. Grushin, F. de Juan, and F. Pollmann, *Phys. Rev. B* **92**, 085147 (2015).
- ⁵⁶ Y. Tomita and Y. Okabe, *Phys. Rev. B* **66**, 180401 (2002).
- ⁵⁷ J. Cardy, *Finite-size scaling*, Vol. 2 (Elsevier, 2012).
- ⁵⁸ M. El-Comorini, A. C. Di Lorenzo, and E. Vicari, *Phys. Rev. B* **89**, 094516 (2014).
- ⁵⁹ O. Melchert, arXiv:0910.5403 (2009).
- ⁶⁰ A. H. MacDonald, S. M. Girvin, and D. Yoshioka, *Phys. Rev. B* **37**, 9753 (1988).
- ⁶¹ F. H. Kim, K. Penc, P. Nataf, and F. Mila, *Phys. Rev. B* **96**, 205142 (2017).
- ⁶² S. Xu, J. Barreiro, Y. Wang, and C. Wu, arXiv:1707.01463 (2017).
- ⁶³ M. Takahashi, *Journal of Physics C: Solid State Physics* **10**, 1289 (1977).